Synthesis and Stereophysical Characterization of the Fischer–Palm-Related 49-Electron Thiocarbonyl-Capped Triangular Nickel Clusters $Ni_3(\eta^5\text{-}C_5H_{5-x}Me_x)_3(\mu_3\text{-}X)(\mu_3\text{-}Y)$ (x = 0, 1), Containing π-Acceptor X and Y Capping Ligands (X = Y = CS; X = CS, Y = CO): Comparative Experimental/Theoretical Analysis of the Triply Bridging Carbonyl and Thiocarbonyl Ligands in Analogous Molecular Environments

Terry E. North,[1a,b] James B. Thoden,[1a,c] Brock Spencer,[1d] Asgeir Bjarnason,[1e] and Lawrence F. Dahl*,[1a]

Department of Chemistry, University of Wisconsin—Madison, Madison, Wisconsin 53706, Department of Chemistry, Beloit College, Beloit, Wisconsin 53511, and Science Institute, University of Iceland, Dunhaga 3, IS-107 Reykjavik, Iceland

Received July 28, 1992

Four new thiocarbonyl-capped analogues of the classic Fischer–Palm 49-electron $Ni_3Cp_3(\mu_3\text{-}CO)_2$ (**1a**, where Cp = η^5-C_5H_5) and the corresponding methylcyclopentadienyl $Ni_3Cp'_3(\mu_3\text{-}CO)_2$ (**1**, where Cp' = η^5-C_5H_4Me) have been synthesized in 10–30% yields; these are the Cp-containing $Ni_3Cp_3(\mu_3\text{-}CS)(\mu_3\text{-}CO)$ (**2a**) and $Ni_3Cp_3(\mu_3\text{-}CS)_2$ (**3a**) and the corresponding Cp'-containing derivatives (**2** and **3**). X-ray diffraction, spectroscopic (IR, UV–vis), ESR, mass spectrometric, and electrochemical measurements of these compounds have provided an unprecedented opportunity for a systematic stereophysical/bonding comparison of the rare capping μ_3-CS ligand with the common capping μ_3-CO ligand in analogous molecular environments. Crystallographic determinations of these triangular nickel thiocarbonyl clusters showed the following salient structural features: (1) equivalent Ni–Ni bond distances in the CS,CO-bicapped **2a** and **2**, which are virtually identical to those in the CO,CO-bicapped **1a** and **1** and only slightly longer (viz., 0.014–0.025 Å) than those in the CS,CS-bicapped **3a** and **3**; (2) the Cp'-containing **2** of crystallographic C_1-1 site symmetry possessing a crystal-ordered pseudo-C_{3v} $Ni_3(CS)(CO)$ core with significantly shorter Ni–CS bond lengths (mean, 1.918 Å) than Ni–CO bond lengths (mean, 1.948 Å) in accordance with stronger Ni–CS bonding; (3) the C–S bond length of 1.598 (2) Å in **2** being significantly longer than that of 1.539 (11) Å in the crystal-ordered pseudo-D_{3h} $Ni_3(CS)_2$ core in **3a**. Laser-desorption/FT mass spectra of **1–3** display parent ion peaks, $[M]^+$, with the most prominent ion peak, $[M - CO]^+$, in **2** involving a preferential loss of CO (with retention of CS). Cyclic voltammograms of **1–3** in CH_2Cl_2 were found to exhibit a one-electron oxidation to the 48-electron monocation and a one-electron reduction to the 50-electron monoanion. A comparison of the $E_{1/2}$ values in these reversible or quasi-reversible redox processes shows that each substitution of CS for CO makes oxidation more difficult (i.e., more positive $E_{1/2}$) and reduction easier (i.e., less negative $E_{1/2}$). The nonparametrized Fenske–Hall model was used to perform MO calculations on **1a**, **2a**, and **3a**. The results of these MO calculations were correlated with the spectroscopic (IR, UV–vis) and ESR data. It was concluded for these closely related electron-rich trimetal clusters that a capping CS ligand (relative to a capping CO ligand) is a much better π*-acceptor and an equivalent σ-donor; in sharp contrast with CO, it is also a weak π-donor.

Introduction

In 1958 Fischer and Palm[2] reported the synthesis and characterization by infrared, dipole moment, and magnetic susceptability measurements of a tricyclopentadienyltrinickel dicarbonyl compound, $Ni_3Cp_3(CO)_2$ (where Cp denotes η^5-C_5H_5). The proposed geometry with one carbonyl ligand capping each side of an equilateral triangle of bonding nickel atoms was ascertained from an X-ray diffraction study by Hock and Mills[3] in 1961. This CO,CO-bicapped triangular metal cluster, now formulated as $Ni_3Cp_3(\mu_3\text{-}CO)_2$, was of particular importance in two ways: (1) it provided the first example of a triply bridging carbonyl ligand; (2) it was unprecedented as a stable paramagnetic triangular metal cluster containing one unpaired electron. Experimental and theoretical studies were thereafter performed on $Ni_3Cp_3(\mu_3\text{-}CO)_2$ to determine the nature of the unpaired electron in this prototypical 49-electron cluster. From ESR measurements, Longuet-Higgins and Stone[4] in 1962 suggested that the unpaired electron occupies a nondegenerate a_2'' HOMO (under D_{3h} symmetry) mainly composed of *trimetal-bonding out-of-plane* Ni d_π AOs. However, subsequent single-crystal ESR investigations by Strouse and Dahl[5] of the paramagnetic $Co_3(CO)_9(\mu_3\text{-}X)$ (X = S, Se)[5-8] doped in the corresponding

(1) (a) University of Wisconsin—Madison. (b) Present address: Molecular Design Ltd., Parsippany, NJ 07054. (c) Present address: Institute for Enzyme Research, University of Wisconsin—Madison. (d) Beloit College. (e) Science Institute, University of Iceland.

(2) Fischer, E. O.; Palm, C. *Chem. Ber.* **1958**, *91*, 1725–1731.

(3) Hock, A. A.; Mills, O. S. In *Advances in the Chemistry of Coordination Compounds*, Kirschner, S., Ed.; Macmillan: New York, 1961; pp 640–648.

(4) Longuet-Higgins, H. C.; Stone, A. *J. Mol. Phys.* **1962**, *5*, 417–425.

(5) (a) Strouse, C. E.; Dahl, L. F. *Discuss. Faraday Soc.* **1969**, *No. 47*, 93–106. (b) Strouse, C. E.; Dahl, L. F. *J. Am. Chem. Soc.* **1971**, *93*, 6032–6041.

(6) (a) Markó, L.; Bor, G.; Klumpp, E.; Markó, B.; Almásy, G. *Chem. Ber.* **1963**, *96*, 955–964. (b) Markó, L.; Bor, G.; Klumpp, E. *Chem. Ind. (London)* **1961**, 1491–1492.

(7) Khattab, S. A.; Markó, L.; Bor, G.; Markó, B. *J. Organomet. Chem.* **1964**, *1*, 373–376.

0276-7333/92/2311-4326$03.00/0

diamagnetic $FeCo_2(CO)_9(\mu_3\text{-}X)$ hosts (X = S, Se)[5,7] unequivocally established that the unpaired electron in each of these monocapped triangular metal clusters occupies a nondegenerate a_2 HOMO (under C_{3v} symmetry) consisting primarily of *trimetal-antibonding in-plane* Co $3d_{xy}$ AOs. From electronic considerations Strouse and Dahl[5a] proposed that the unpaired electron in the electronically equivalent Fischer–Palm $Ni_3Cp_3(\mu_3\text{-}CO)_2$ occupies the corresponding *trimetal-antibonding* a_2' HOMO (under D_{3h} symmetry). Later "quantum mechanical" experimental analyses[9] involving stereochemical and magnetic susceptibility measurements of its monoanion and cobalt–dinickel analogues of its monocation provided a self-consistent metal cluster bonding model that substantiated the Strouse–Dahl proposal that the unpaired electron in $Ni_3Cp_3(\mu_3\text{-}CO)_2$ resides in the trimetal-antibonding a_2' HOMO. Theoretical calculations[10,11] have corroborated this assignment of the HOMO in $Ni_3Cp_3(\mu_3\text{-}CO)_2$. Since the isolation of the classic Fischer–Palm molecule, a large number of metal clusters containing triply bridging carbonyl ligands have been prepared and structurally characterized.

Although a wide variety of compounds with terminal and doubly bridging thiocarbonyl ligands have also been synthesized and extensively studied,[12] the only known compounds possessing a triply bridging CS ligand (prior to a preliminary report[13] of this work) are the 48-electron $Co_3Cp_3(\mu_3\text{-}CS)(\mu_3\text{-}S)$ prepared and crystallographically characterized by Werner et al.[14] and the mixed Cp′/Cp-substituted $Co_3Cp_{3-x}Cp'_x(\mu_3\text{-}CS)(\mu_3\text{-}S)$ analogues (x = 0, 1, 2) prepared and spectroscopically characterized by Fortune and Manning.[15] Unfortunately, reliable molecular parameters were not obtained in the X-ray diffraction study[14] of $Co_3Cp_3(\mu_3\text{-}CS)(\mu_3\text{-}S)$ due to a crystal disorder in which the capping CS and S ligands in each of the two independent molecules are superimposed on each other by reflection across a pseudo-horizontal mirror plane containing the cobalt atoms.[16,17] Our efforts[18] to prepare a crystal-ordered methylcyclopentadienyl analogue of the 53-electron $Ni_3Cp_3(\mu_3\text{-}S)_2$[19] by reaction of $Ni_2Cp'_2(\mu\text{-}CO)_2$ with CS_2 resulted instead in the isolation of $Ni_3Cp'_3(\mu_3\text{-}CS)(\mu_3\text{-}CO)$ (**2**) and $Ni_3Cp'_3(\mu_3\text{-}CS)_2$ (**3**, where Cp′ denotes $\eta^5\text{-}C_5H_4Me$). This discovery of a convenient synthetic route for obtaining thiocarbonyl-substituted derivatives of the known Cp′ analogue, $Ni_3Cp'_3(\mu_3\text{-}CO)_2$ (**1**),[20] of the Fischer–Palm molecule (**1a**) provided the incentive to synthesize the corresponding cyclopentadienyl $Ni_3Cp_3(\mu_3\text{-}CS)(\mu_3\text{-}CO)$ (**2a**) and $Ni_3Cp_3(\mu_3\text{-}CS)_2$ (**3a**) by an analogous reaction. These four closely related thiocarbonyl-capped trinickel clusters (**2**, **3**, **2a**, **3a**) and their dicarbonyl-capped counterparts (**1**, **1a**) have formed the basis for a systematic crystallographic/spectroscopic/electrochemical examination (presented herein) in order to compare the rare capping μ_3-CS ligand with the common capping μ_3-CO ligand in analogous molecular environments.

We have also carried out MO calculations on **1a**, **2a**, and **3a** with the parameter-free Fenske–Hall model.[21] Although Fenske–Hall MO calculations on the Fischer–Palm **1a** had been previously reported by Rives et al.,[11] we decided to repeat the calculations in order to use the same basis functions (vide infra) for **1a**, **2a**, and **3a** and thereby to ensure a valid comparative theoretical analysis; it is noteworthy that the results from the Fenske–Hall method[21] are dependent upon the choice of basis set.[22]

The electronic structure of "free" thiocarbonyl has been previously investigated by an ab initio calculation[23] and by use of the approximate Fenske–Hall MO method.[24] These calculations along with the Fenske–Hall calculations and photoelectron spectral measurements by Lichtenberger and Fenske[24] on $Cr(CO)_5CS$ and $MnCp(CO)_2CS$, in which the terminal CS ligand has been substituted in place of a terminal CO one, indicate that CS should be both a better π-acceptor and a better σ-donor ligand than CO. In addition, the latter calculations[24] led to the prediction that CS may also function as a π-donor ligand. In the MO calculations presented herein, the bonding of the μ_3-CS and μ_3-CO ligands is examined in analogous molecular environments in **1a**, **2a**, and **3a**. These MO results are correlated with the observed experimental trends obtained from the physical characterization of these compounds.

Experimental Section

General Techniques and Materials. Work was done with the rigorous exclusion of air and water. Reactions and manipulations were carried out under an atmosphere of nitrogen that had been dried by passage through an Aquasorb column. Standard Schlenk-type apparatus and techniques were employed, with either a preparative vacuum line or a Vacuum Atmospheres drybox. The following solvents were dried and freshly distilled under N_2 prior to use: carbon disulfide (CaH_2), cyclopentane (Na, anthracene), dichloromethane (CaH_2), hexane (CaH_2), THF (K, benzophenone), and toluene (Na). Benzene was used as received. All deuterated NMR solvents were predried over activated 3-Å molecular sieves, frozen and degassed three times, and then vacuum-distilled before use. Alumina was obtained from Aldrich (activated, neutral, Brockmann Activity I, ~150 mesh) and stored in a 110 °C oven prior to use. Silica gel, obtained from E.M. Science (230–400 mesh; denoted as Silica Gel 60), was predried at 150 °C for 24 h under vacuum and then deactivated with 5% degassed water before use. All other reagents were purchased from major suppliers and used without further purification. Proton NMR data were obtained with a Bruker WP-200 FT-NMR

(8) (a) Wei, C. H.; Dahl, L. F. *Inorg. Chem.* **1967**, *6*, 1229–1236. (b) Stevenson, D. L.; Wei, C. H.; Dahl, L. F. *J. Am. Chem. Soc.* **1971**, *93*, 6027–6031.

(9) (a) Byers, L. R.; Uchtman, V. A.; Dahl, L. F. *J. Am. Chem. Soc.* **1981**, *103*, 1942–1951. (b) Maj, J. J.; Dahl, L. F. *J. Am. Chem. Soc.* **1982**, *104*, 3054–3063.

(10) (a) Schilling, E. R.; Hoffmann, R. *J. Am. Chem. Soc.* **1979**, *101*, 3456–3467. (b) Pinhas, A. R.; Albright, T. A.; Hofmann, P.; Hoffmann, R. *Helv. Chim. Acta* **1980**, *63*, 29–49.

(11) Rives, A. B.; You, X.-Z.; Fenske, R. F. *Inorg. Chem.* **1982**, *21*, 2286–2294.

(12) (a) Broadhurst, P. V. *Polyhedron* **1985**, *4*, 1801–1846. (b) Yaneff, P. V. *Coord. Chem. Rev.* **1977**, *23*, 183–220. (c) Butler, I. S.; Fenster, A. E. *J. Organomet. Chem.* **1974**, *66*, 161–194. (d) Butler, I. S. *Acc. Chem. Res.* **1977**, *10*, 359–365. (e) Butler, I. S. *Pure Appl. Chem.* **1988**, *60*, 1241–1244.

(13) North, T. E.; Spencer, B.; Harris, H. A.; Dahl, L. F. *Abstracts of Papers*, 196th National Meeting of the American Chemical Society, Los Angeles, CA, Sept 1988; American Chemical Society: Washington, D.C., 1988.

(14) (a) Werner, H.; Leonhard, K. *Angew. Chem., Int. Ed. Engl.* **1979**, *18*, 627–628. (b) Werner, H.; Leonhard, K.; Kolb, O.; Röttinger, E.; Vahrenkamp, H. *Chem. Ber.* **1980**, *113*, 1654–1662.

(15) Fortune, J.; Manning, A. R. *Organometallics* **1983**, *2*, 1719–1723.

(16) The synthesis and structure of a crystal-ordered 48-electron heterometallic analogue, $(PPh_3)(CO)_2FeCo_2Cp_2(\mu_3\text{-}CS)(\mu_3\text{-}S)$, in which an isolobal $Fe(PPh_3)(CO)_2$ fragment has been formally inserted in place of a CoCp fragment, were recently reported by Manning et al.[17] The triply bridging CS ligand coordinated to the $FeCo_2$ triangle has a C–S bond length of 1.646 (3) Å and Fe–CS and Co–CS bond lengths of 2.078 (3) and 1.913 (4) Å, respectively; it was stated[17] that an IR band at 1020 cm^{-1} may be due to the ν(CS) mode.

(17) Manning, A. R.; O'Dwyer, L.; McArdle, P. A.; Cunningham, D. *J. Chem. Soc., Chem. Commun.* **1992**, 897–898.

(18) North, T. E.; Thoden, J. B.; Spencer, B.; Bjarnason, A.; Dahl, L. F., submitted to *Organometallics*.

(19) Vahrenkamp, H.; Uchtman, V. A.; Dahl, L. F. *J. Am. Chem. Soc.* **1968**, *90*, 3272–3273.

(20) Englert, M. H. Ph.D. Thesis, University of Wisconsin—Madison, 1983.

(21) Hall, M. B.; Fenske, R. F. *Inorg. Chem.* **1972**, *11*, 768–775.

(22) Fenske, R. F. *Pure Appl. Chem.* **1988**, *60*, 1153–1162.

(23) Richards, W. G. *Trans. Faraday Soc.* **1967**, *63*, 258–261.

(24) Lichtenberger, D. L.; Fenske, R. F. *Inorg. Chem.* **1976**, *15*, 2015–2022.

Table I. Comparison of Triply Bridging Carbonyl and Thiocarbonyl Infrared Stretching Frequencies in the Solid State (KBr Pellet) for $Ni_3Cp'_3(\mu_3\text{-}CO)_2$ (1), $Ni_3Cp_3(\mu_3\text{-}CO)_2$ (1a), $Ni_3Cp'_3(\mu_3\text{-}CS)(\mu_3\text{-}CO)$ (2), $Ni_3Cp_3(\mu_3\text{-}CS)(\mu_3\text{-}CO)$ (2a), $Ni_3Cp'_3(\mu_3\text{-}CS)_2$ (3), and $Ni_3Cp_3(\mu_3\text{-}CS)_2$ (3a)

freq, cm^{-1}	1	1a	2	2a	3	3a
ν_{CO}	1735	1733	1763	1765		
ν_{CS}			1128	1135	1101	1105

spectrometer. Shifts were referenced indirectly to TMS via residual proton signals in the deuterated solvent. $Ni_2Cp_2(\mu_2\text{-}CO)_2$ and $Ni_2Cp'_2(\mu_2\text{-}CO)_2$ were prepared by the method of King[25] by reactions of nickel tetracarbonyl with nickelocene and bis(methylcyclopentadienyl)nickel, respectively, in refluxing benzene. The unsubstituted and methyl-substituted nickelocenes for the above procedures were synthesized by the method of Cordes.[26]

Synthesis. (a) Reaction of $Ni_2Cp'_2(\mu_2\text{-}CO)_2$ with CS_2. In a typical preparation, 1.00 g (3.01 mmol) of $Ni_2Cp'_2(\mu_2\text{-}CO)_2$ was slowly added to 75 mL of CS_2 under a N_2 purge. The solution was refluxed for 1 h, at which time an IR spectrum showed that all the nickel dimer had been consumed. During the course of the reaction, the solution turned from red to brown. After the CS_2 was removed in vacuo, the solid products were exhaustively extracted with toluene and then with THF; a black residue of NiS remained.

The toluene extracts were combined, reduced in volume, and loaded onto a chromatographic column containing oxygen-free alumina packed with hexane and maintained under nitrogen. Elution with toluene separated three closely spaced bands: band 1, the dark red $Ni_3Cp'_3(\mu_3\text{-}CS)_2$ (3); band 2, the reddish-brown $Ni_3Cp'_3(\mu_3\text{-}CS)(\mu_3\text{-}CO)$ (2); and band 3, the yellow-brown $Ni_3Cp'_3(\mu_3\text{-}CO)_2$ (1). The remaining black material could not be removed from the column. All of these bands were further purified by chromatography on a smaller silica gel column packed with toluene under nitrogen. Elution with toluene and subsequent removal of the solvent gave crystalline material in the following estimated yields: 3, ~10%; 2, ~30%; 1, ~20%.

The THF extract yielded $[Ni_3Cp'_3]_2(C_2S_6)$ (4, ~2%), which is discussed in the following paper.[27]

(b) Reaction of $Ni_2Cp_2(\mu_2\text{-}CO)_2$ with CS_2. This reaction was carried out in a manner similar to that for the Cp′ analogue as described above. In this case, a 2-h reflux was required for complete reaction of the dimeric nickel cyclopentadienyl starting material. The same separation and purification procedure was followed that yielded the Cp′ analogues (1–3). Estimated yields and the order of isolation were dark red $Ni_3Cp_3(\mu_3\text{-}CS)_2$ (3a, ~10%), reddish-brown $Ni_3Cp_3(\mu_3\text{-}CS)(\mu_3\text{-}CO)$ (2a, ~30%), and yellow-brown $Ni_3Cp_3(\mu_3\text{-}CO)_2$ (1a, ~20%).

Characterization of the Triangular Metal Systems. (a) Physical Properties. The colors of these species are as follows: 1 and 1a are yellow-brown, 2 and 2a are reddish brown, and 3 and 3a are dark red. 1–3 are moderately air-stable in the solid state but decompose slowly in solution when exposed to oxygen. The air-instability increases with increasing CS substitution. 1–3 are soluble in all the solvents tested, which ranged in polarity from pentane to acetone. The unsubstituted Cp analogues (1a–3a) are soluble in polar solvents but only moderately soluble in toluene. As expected for paramagnetic species, all of these 49-electron trimetal clusters do not exhibit a ^1H NMR signal.

(b) Infrared Data. Solid-state infrared spectra were obtained with a Mattson FT-IR spectrophotometer. Carbonyl and thiocarbonyl stretching frequencies for $Ni_3Cp'_3(\mu_3\text{-}CO)_2$ (1), $Ni_3Cp_3(\mu_3\text{-}CO)_2$ (1a), $Ni_3Cp'_3(\mu_3\text{-}CS)(\mu_3\text{-}CO)$ (2), $Ni_3Cp_3(\mu_3\text{-}CS)(\mu_3\text{-}CO)$ (2a), $Ni_3Cp'_3(\mu_3\text{-}CS)_2$ (3), and $Ni_3Cp_3(\mu_3\text{-}CS)_2$ (3a) in the solid state (KBr pellet) are summarized in Table I.

(c) UV–Vis Data. UV–vis spectra were obtained with a Perkin-Elmer Lambda Array 3840 spectrophotometer. Quartz sample cells of 1.0-cm path length were used; all spectra were recorded at room temperature in hexane and corrected for solvent background. Electronic transitions for the two major bands observed for 1–3 in the visible region are given in Table II.

Table II. Comparison of the Two Lowest Energy Visible Absorption Band-Maxima for the Three Members (X = Y = CO (1); X = CS, Y = CO (2); X = Y = CS (3)) of the $Ni_3Cp'_3(\mu_3\text{-}X)(\mu_3\text{-}Y)$ Series with Calculated Values of Assigned Electronic Transitions Obtained via Fenske–Hall MO Calculations

species (X)(Y)	band[a]	λ_{max}, nm	ΔE_{max}, eV	ΔE_{calc}, eV
1 (CO)(CO)	A	590	2.10	1.95
	B	456	2.72	2.62
2(CS)(CO)	A	690	1.80	1.50
	B	476	2.60	2.48
3 (CS)(CS)	A	710	1.75	1.31
	B	500	2.48	2.11

[a] Under D_{3h} symmetry, band A is assigned to the $A'_2 \rightarrow E''$ transition and band B to the $A'_2 \rightarrow E'$ transition.

(d) ESR Data. ESR studies were carried out on a Varian E-15 ESR spectrometer. DPPH was used as a standard for g-value determinations. Glass samples were prepared by rapidly quenching dilute solutions in liquid nitrogen; low-temperature spectra were checked for possible power saturation. ESR spectra of 1–3 in cyclopentane solution at room temperature gave nearly identical line widths of approximately 40 G with $g_{av} = 2.05$ for each species. In cyclopentane glass matrices at 98 K, the ESR spectra exhibited virtually identical line shapes expected for an axially symmetric spin $^1/_2$ system with the following g values: $g_\parallel = 2.02$, $g_\perp = 2.10$ for 1, $g_\parallel = 2.02$, $g_\perp = 2.10$ for 2, $g_\parallel = 2.02$, $g_\perp = 2.11$ for 3.

(e) Mass Spectral Data. Mass spectra were obtained with an EXTREL FTMS-2000 laser desorption Fourier transform (LD/FT) mass spectrometer (EXTREL FTMS, Madison, WI) equipped with a 3.0-T superconducting magnet; desorption of each sample was achieved with a CO_2 laser and an EXTREL LD interface. Additional details concerning the FTMS-2000 instrument and procedures for sample preparation and data collection are available elsewhere.[28]

Positive-ion LD/FT mass spectra of the methylcyclopentadienyl 1–3 exhibit a number of structurally consistent high-mass ion peaks including the parent ion peaks. The mass spectrum of 1 displays signals assigned to the following ion fragments (with intensities relative to the base peak as 100): m/z 469 (parent ion $[M]^+ = [Ni_3Cp'_3(CO)_2]^+$, 18), 441 ($[M - CO]^+$, 55), 411 ($[M - 2CO - 2H]^+$, 47), 407 ($[M - 2CO - 6H]^+$, 100), 272 ($[Ni_2Cp'_2 - 2H]^+$, 12), 216 ($[NiCp'_2]^+$, 50), and 136 ($[NiCp' - H]^+$, 14). Prominent signals in the mass spectrum of 2 include: m/z 485 (parent ion $[M]^+ = [Ni_3Cp'_3(CS)(CO)]^+$, 16), 457 ($[M - CO]^+$, 100), 441 ($[M - CS]^+$, 13), and 216 ($[NiCp'_2]^+$, 18). Assigned peaks in the mass spectrum of 3 are m/z 501 (parent ion $[M]^+ = [Ni_3Cp'_3(CS)_2]^+$, 100), 467 ($[M - S - 2H]^+$, 8), 421 ($[M - Cp' - H]^+$, 6), 387 ($[M - Cp' - S - 3H]^+$, 19), and 216 ($[NiCp'_2]^+$, 5).

(f) Electrochemical Data. Cyclic voltammograms (CVs) were carried out with a BAS-100 electrochemical analyzer connected to a PAR electrochemical cell inside a Vacuum Atmospheres drybox under an atmosphere of purified nitrogen. The three-electrode cell was comprised of a platinum disk working electrode, a platinum wire counter electrode, and a reference saturated calomel electrode. A 0.1 M tetra-n-butylammonium hexafluorophosphate solution was used as the supporting electrolyte. Additional details of the cell configuration and experimental method are given elsewhere.[29] An iR compensation was made for solution resistance, and linear sweep voltammetry (LSV) was used to verify the direction of electron transfer (oxidation or reduction). Half-wave potentials ($E_{1/2}$) were calculated based on the equation $E_{1/2} = (E_{pa} + E_{pc})/2$, where E_{pa} is the anodic peak potential and E_{pc} is the cathodic peak potential. The degree of electrochemical reversibility was determined from the near-unity values of the peak-current ratio (i_a/i_c) and the near-independence

(25) King, R. B. *Organometallic Synthesis*; Academic: New York, 1965; Vol. 1, pp 119–121.
(26) Cordes, J. F. *Chem. Ber.* **1962**, *95*, 3084–3085.
(27) North, T. E.; Thoden, J. B.; Dahl, L. F. *Organometallics*, following paper in this issue.
(28) (a) Bjarnason, A.; DesEnfants, II, R. E.; Barr, M. E., Dahl, L. F. *Organometallics* **1990**, *9*, 657–661. (b) Bjarnason, A. *Rapid Commun. Mass Spectrom.* **1989**, *3*, 373–376.
(29) Bedard, R. L.; Dahl, L. F. *J. Am. Chem. Soc.* **1986**, *108*, 5933–5942.

Table III. Electrochemical Data on 49-Electron $Ni_3Cp'_3(\mu_3\text{-}CO)_2$ (1), $Ni_3Cp'_3(\mu_3\text{-}CS)(\mu_3\text{-}CO)$ (2), and $Ni_3Cp'_3(\mu_3\text{-}CS)_2$ (3) in CH_2Cl_2 and THF

	E_p,[b] V	$E_{1/2}$, V	ΔE_p, mV	i_{pa}/i_{pc}	assign[c]
(a) CH_2Cl_2					
0 → 1+					
1[d]	+0.34	+0.30	78	1.00	rev
2	+0.41	+0.37	78	1.92	quasi
3	+0.47	+0.42	96	0.97	rev
0 → 1-					
1[d]	−1.05	−1.02	72	1.00	rev
2	−0.91	−0.86	97	0.67	quasi
3	−0.82	−0.77	109	0.83	rev
(b) THF					
0 → 1+					
1	+0.44	+0.37	141	0.84	quasi
2	+0.48				irrev
3	+0.53	+0.48	94	1.16	rev
0 → 1-					
1	−1.06	−1.00	121	1.20	quasi
2	−0.95	−0.88	148	1.07	quasi
3	−0.80	−0.75	98	1.01	rev

[a] The scan rate is 200 mV/s. [b] Anodic peak potentials are given for oxidations and cathodic peak potentials are given for reductions. [c] Criteria used for assignment of reversibility, quasi-reversibility, and irreversibility are peak current ratios and dependence of ΔE_p on changes in scan rate. [d] See refs 20 and 29.

of the separation between anodic and cathodic peak potentials (ΔE_p) with changes in scan rate. Electrochemical data for **1–3** are summarized in Table III.

(g) Elemental Analysis. The stoichiometry of each of the two thiocarbonyl-capped methylcyclopentadienyl nickel clusters $Ni_3Cp'_3(\mu_3\text{-}CS)(\mu_3\text{-}CO)$ (**2**) and $Ni_3Cp'_3(\mu_3\text{-}CS)_2$ (**3**) is in accordance with elemental analysis (Galbraith Laboratories, Inc). Analysis Calcd (found) for $Ni_3SOC_{20}H_{21}$ (**2**): Ni, 36.27 (35.72); S, 6.60 (6.48); C, 49.47 (48.81); H, 4.36 (4.02). Calcd (found) for $Ni_3S_2C_{20}H_{21}$ (**3**): Ni, 35.11 (34.69); S, 12.78 (12.11); C, 47.89 (47.42); H, 4.22 (3.98).

Nonparametrized Fenske–Hall Molecular Orbital Calculations. (a) General Comments. Calculations were performed on **1a**, **2a**, and **3a** with the Fenske–Hall molecular orbital model.[21] This model is based on a self-consistent-field method, which is an approximation of the Hartree–Fock–Roothaan procedure. There are no adjustable or empirical parameters so that the resulting eigenvalues and eigenvectors are completely determined by the input geometry and by the nature of the basis functions. A detailed description of this method and examples of its applications are given elsewhere.[22,30,31]

(b) Basis Functions. Clementi's free-atom double-ζ Hartree–Fock Slater type orbitals (STOs)[32] were used for C, O, and S. All but the valence shell p functions were curve fit to single-ζ form using the criterion of maximum overlap.[33] A value of 1.16 was used for the exponent on the hydrogen 1s AO. Nickel (+1) AO functions were taken from Richardson et al.;[34] these functions were all of single-ζ form except for the 3d functions, which were of double-ζ form. The exponents for the single-ζ 4s and 4p AOs were arbitrarily set at 2.0.

(c) Geometries. Idealized D_{3h} molecular geometries for $Ni_3Cp_3(\mu_3\text{-}CO)_2$ (**1a**) and $Ni_3Cp_3(\mu_3\text{-}CS)_2$ (**3a**) and an idealized C_{3v} molecular geometry for $Ni_3Cp_3(\mu_3\text{-}CS)(\mu_3\text{-}CO)$ (**2a**) are based on X-ray crystallographic data for the methylcyclopentadienyl **1** and **2**, which have C_1-1 site symmetry. These point groups assume that each Cp ring has cylindrical symmetry; in fact, calculations with the Cp ligands rotated to various orientations produced negligible changes in the results. The Cp configuration used has the centroid of each pentagonal D_{5h} ring lying in the plane formed by the three nickel atoms with one carbon vertex of the regular carbon pentagon perpendicular to the trinickel plane. The idealized geometries conform to the following identical mean bond distances: Ni–Ni, 2.39 Å; Ni–CO, 1.94 Å; Ni–CS, 1.91 Å; C–O, 1.18 Å; C–S, 1.60 Å; Ni–C(ring), 2.11 Å; C(ring)–C(ring), 1.41 Å.

(d) General Considerations. Calculations were first carried out on the ligands alone in order to transform the atomic orbital basis set into a basis set composed of molecular orbitals. The eigenvectors resulting from these ligand transformations were then used as basis sets for the Cp rings and the bridging CS and CO ligands in the calculation on each composite molecule. This allows the results to be analyzed in terms of a free-ligand basis set as well as free-atom orbitals. The bonding picture obtained is greatly simplified, but the numerical results remain unchanged. Additional preliminary calculations were also performed on the Ni_3Cp_3 fragments, which were later introduced into each composite calculation in the same manner. The numerical results from calculations with different fragment components all agreed with each other and with the results from calculations performed with a completely free-atom basis where no preliminary transformations were performed. When shown on the same correlation diagram with the total complex, the energies of the fragment molecular orbitals are the diagonal elements of the Fock matrices for the entire complex.

The low-lying occupied σ orbitals of each ligand for which a transformed basis set was employed (viz., the three Cp rings and the CS and CO ligands) were frozen out of the calculation as ligand core orbitals. Thus, the five C–C and five C–H σ-bonding orbitals for each Cp ring and the 3σ orbital for the CO and the 6σ orbital for the CS were deleted (along with the associated virtual orbitals) from the SCF solution. This method is used to avoid possible counterintuitive orbital mixing.[22,35] The merits of this treatment of ligand core orbitals are given elsewhere.[24,36–38] All calculations were performed with each cyclopentadienyl ligand treated as a closed-shell monoanion. To maintain consistency with the molecular charge, a Ni(+1) basis set was used.

X-ray Crystallographic Studies. (a) General Comments. Each crystal was immobilized with epoxy glue inside an argon-filled Lindemann glass capillary, which was then flame-sealed. Intensity data were collected at ambient temperature (20 °C) on a Siemens P3/F diffractometer with graphite-monochromated Mo Kα radiation (λ = 0.7107 Å). Refined lattice constants were determined from a least-squares analysis of 25 well-centered high-angle reflections. Axial photographs were used to confirm lattice lengths and cell symmetry. All calculations were performed on a DEC MicroVax II system with the SHELXTL-Plus program package. All data were corrected for absorption using empirical absorption corrections based on Ψ-scans applied to each data set before the structural solution was attempted. Crystallographic data and refinement parameters are listed in Table IV for **2**, **2a**, **3**, and **3a**. Neutral atomic scattering factors were used with anomalous dispersion corrections for all nonhydrogen atoms. Idealized atomic positions were calculated for the hydrogen atoms, which in the least-squares refinement were treated as fixed-atom contributors. Tables of positional parameters and equivalent isotropic thermal parameters, anisotropic thermal parameters, selected interatomic distances and bond angles, and parameters for hydrogen atoms are available for each crystal structure (**2**, **2a**, **3**, and **3a**) as supplementary material (see paragraph at end of paper).

(b) $Ni_3Cp'_3(\mu_3\text{-}CS)(\mu_3\text{-}CO)$ (2). Dark green single crystals of **2** were grown from a slowly evaporating hexane solution under N_2. A parallelepiped-shaped crystal of approximate dimensions 0.80 × 0.45 × 0.30 mm was selected for data collection. The triclinic crystal structure was found to conform to centrosymmetric $P\bar{1}$ symmetry with the two molecules in the unit cell related by

(30) (a) Fenske, R. F. *Prog. Inorg. Chem.* **1976**, *21*, 179–208. (b) Fenske, R. F. *Pure Appl. Chem.* **1971**, *27*, 61–71.
(31) Harris, H. A.; Kanis, D. R.; Dahl, L. F. *J. Am. Chem. Soc.* **1991**, *113*, 8602–8611 and references therein.
(32) Clementi, E.; Ramondi, D. L. *J. Chem. Phys.* **1963**, *38*, 2686–2689.
(33) Radtke, D. D. Ph.D. Thesis, University of Wisconsin—Madison, 1966.
(34) Richardson, J. W.; Nieuwport, W. C.; Powell, R. R.; Edgell, W. F. *J. Chem. Phys.* **1962**, *36*, 1057–1061.
(35) (a) Whangbo, M.-H.; Hoffmann, R. *J. Chem. Phys.* **1978**, *68*, 5498–5500. (b) Ammeter, J. H.; Burgi, H.-B.; Thibeault, J. C.; Hoffmann, R. *J. Am. Chem. Soc.* **1978**, *100*, 3686–3692.
(36) Petersen, J. L.; Lichtenberger, D. L.; Fenske, R. F.; Dahl, L. F. *J. Am. Chem. Soc.* **1975**, *97*, 6433–6441.
(37) (a) Lichtenberger, D. L.; Fenske, R. F. *J. Am. Chem. Soc.* **1976**, *98*, 50–63. (b) Lichtenberger, D. L.; Fenske, R. F. *J. Chem. Phys.* **1976**, *64*, 4247–4264.
(38) See footnote 31 in ref 31.

Table IV. Crystallographic Data and Refinement Parameters for $Ni_3Cp'_3(\mu_3\text{-}CS)(\mu_3\text{-}CO)$ (2), $Ni_3Cp_3(\mu_3\text{-}CS)(\mu_3\text{-}CO)$ (2a), $Ni_3Cp'_3(\mu_3\text{-}CS)_2$ (3), and $Ni_3Cp_3(\mu_3\text{-}CS)_2$ (3a)

	2	2a	3	3a
formula wt, g/mol	485.5	443.5	501.6	459.5
cryst syst	triclinic	hexagonal	trigonal	hexagonal
space group	$P\bar{1}$	$P6_3$	$R\bar{3}c$	$P6_3/m$
Z	2	2	6	2
a, Å	9.182 (2)	9.305 (2)	9.324 (1)	9.349 (1)
b, Å	9.224 (1)	9.305 (2)	9.324 (1)	9.349 (1)
c, Å	13.001 (1)	11.233 (2)	40.632 (7)	11.510 (4)
α, deg	84.32 (1)	90	90	90
β, deg	82.59 (2)	90	90	90
γ, deg	62.19 (1)	120	120	120
V, Å^3	964.7 (3)	842.2 (5)	3059.7 (9)	871.2 (4)
d(calcd), g/cm^3	1.67	1.75	1.63	1.75
μ(calcd) cm^{-1}	30.2	34.5	29.5	34.5
data collect temp, °C	20	20	20	20
scan mode	θ–2θ	ω	ω	ω
scan speed, deg/min	var (4–29)	var (4–29)	var (3–29)	var (3–29)
2θ limits, deg	3–55	3–55	3–60	3–50
backgd anal.	profile	profile	profile	profile
no. check reflns/freq	3/47	3/47	3/47	3/47
cutoff for obsd data	$\|F\| > 3.0\sigma(F)$	$\|F\| > 3.0\sigma(F)$	$\|F\| > 3.0\sigma(F)$	$\|F\| > 3.0\sigma(F)$
no. of obsd reflns	4179	564	736	426
no. params refined	227	63	68	66
data/param ratio	18.4/1	9.0/1	10.8/1	6.5/1
$R(F)$[a] %	3.22	5.68	4.91	6.16
$R_w(F)$[b] %	4.91	8.98	4.52	4.51
GOF[c]	1.78	2.40	2.13	1.91

[a] $R(F) = R_1(F) = [\sum(||F_o| - |F_c||)/\sum|F_o|] \times 100$. [b] $R_w(F) = R_2(F) = [\sum w_i(||F_o| - |F_c||)^2/\sum w_i(|F_o|)^2]^{1/2} \times 100$. [c] Goodness-of-fit, GOF = $[\sum w_i(||F_o| - |F_c||)^2/(m-n)]^{1/2}$, where m is the number of independent data and n is the number of variable parameters.

a center of symmetry. The positions of the nickel atoms were located by direct methods, and the other non-hydrogen atoms were determined by successive difference Fourier maps. The ring carbon atoms and methyl carbon substituents for the three independent Cp′ ligands were refined anisotropically without any constraints. A final electron-density difference map did not show any residual electron density peaks greater than 1.0 e/Å^3.

(c) $Ni_3Cp_3(\mu_3\text{-}CS)(\mu_3\text{-}CO)$ (2a). Brown single crystals of **2a** were grown from a slowly evaporating hexane solution under N_2. A parallelepiped-shaped crystal of approximate dimensions 0.80 × 0.80 × 0.55 mm was selected for data collection under hexagonal C_{6h}-6/m Laue symmetry. Observed systematic absences indicated the probable space group as either the centrosymmetric $P6_3/m$ or noncentrosymmetric $P6_3$. A statistical analysis of the data failed to show a preference for either the centrosymmetric or noncentrosymmetric space group, so solution and refinement were attempted in each. The space group $P6_3/m$ imposes crystallographic C_{3h}-3/m site symmetry on each of the two equivalent molecules in the unit cell; thus, the μ_3-CS and μ_3-CO ligands, which lie on a crystallographic 3-fold axis, would be disordered across the horizontal mirror plane that contains the nickel atoms. This crystallographically imposed crystal disorder necessitates equal occupancy factors of 0.5 for the μ_3-CS and μ_3-CO ligands. A better refinement was achieved using the noncentrosymmetric space group $P6_3$, for which the imposed C_3-3 site symmetry results in the crystallographically independent unit consisting of one nickel atom, one μ_3-CS and one μ_3-CO ligand, and one Cp ring.

The position of the independent nickel atom was located by direct methods, and the other non-hydrogen atoms were determined by successive difference Fourier maps. The triply bridging thiocarbonyl and carbonyl ligands were found to be disordered on either side of the trinickel plane. It was necessary to refine these ligands isotropically as rigid groups fixed on the threefold axis. On the basis of numerous trial refinements, the Ni–CS and Ni–CO distances were fixed (by use of the DFIX command in SHELXTL) at 1.92 and 1.97 Å, respectively, and the C–S and C–O distances at 1.58 and 1.17 Å, respectively. The site occupancy factors for the two disordered configurations refined to 75% and 25%. The independent Cp ring was refined anisotropically as a rigid D_{5h} group in one ordered orientation with the ring C–C distance fixed at 1.42 Å. A final electron-density difference map showed no residual electron density peaks greater than 1.0 e/Å^3.

(d) $Ni_3Cp'_3(\mu_3\text{-}CS)_2$ (3). Dark red single crystals of **3** were grown from a slowly evaporating cyclopentane solution at −20 °C under N_2. A parallelepiped-shaped crystal of approximate dimensions 0.50 × 0.45 × 0.61 mm was selected for data collection. The possibility of hexagonal instead of trigonal symmetry was eliminated by examination of the intensity data, which showed that $I(h,k,l) \neq I(h,k,\bar{l})$. A triply-primitive hexagonal unit cell corresponding to the obverse setting of the primitive rhombohedral lattice was chosen on the basis of the occurrence of systematic absences of $hkil$ with $-h + k + l \neq 3n$. The additional systematic absences of $h\bar{h}0l$ with l odd indicated the probable space group to be either the noncentrosymmetric $R3c$ or centrosymmetric $R\bar{3}c$.

The position of the independent nickel atom was determined by direct methods under $R\bar{3}c$ symmetry. However, successive Fourier difference maps revealed the presence of crystal disorder about the 3-fold axis. Structural solutions and attempted refinements under the noncentrosymmetric space group $R3c$ and under possible alternative centrosymmetric space groups $R\bar{3}m$ and $R\bar{3}$, were unsuccessful. An examination of the systematic absences in the intensity-weighted reciprocal lattice (via a SHELXTL program) clearly supported the original choices of $R\bar{3}c$ and $R3c$ as the probable space groups.

The 3-fold-related nickel atoms atoms of **3** were observed to be in three different orientations about a 3-fold axis in the unit cell. Attempts to model this crystal disorder were abandoned after it became obvious that the number of parameters required far exceeded the available data. Best results were obtained by anisotropic refinement of **3** as an averaged structure under $R\bar{3}c$ symmetry. For $Z = 6$, this results in the crystallographically independent unit being composed of one Ni atom, one μ_3-CS ligand, and one Cp′ ligand. In addition to the observed crystal disorder described above, a horizontal crystallographic 2-fold axis passing through each nickel position imposes a twofold rotational disorder on each Cp′ ring. Idealized positions for the carbon and sulfur atoms in the μ_3-CS ligand were calculated from bond distances obtained from **2**. These atoms were allowed to move freely on the threefold axis in the later stages of the refinement. An idealized Cp′ ligand (based on another Cp′-containing structure) was placed in the "cloud" of electron density generated by the extensive Cp′ disorder, which was evidenced by the large residual peaks observed in the difference Fourier maps. The entire independent Cp′ ligand was refined as a rigid group by constraining all ring C–C distances to 1.40 Å and all ring diagonal C···C distances to 2.27 Å. The distance between the methyl carbon and the ring carbon atom to which it is attached was fixed at 1.50 Å. All non-hydrogen atoms were refined anisotropically in the

final cycles. A final electron-density difference map did not reveal any unusual features other than residual disorder present around the Cp′ ligands.

(e) $Ni_3Cp_3(\mu_3\text{-}CS)_2$ (3a). Dark red, single crystals of **3a** were grown from a saturated hexane solution maintained at −20 °C under N_2 for a period of approximately 2 months. A parallelepiped-shaped crystal of approximate dimensions 0.15 × 0.22 × 0.64 mm was selected for data collection.

Observed systematic absences indicated the probable space group to be either the centrosymmetric $P6_3/m$ or noncentrosymmetric $P6_3$. A statistical analysis of the data indicated that the space group was centrosymmetric, and this choice was corroborated by the successful solution and refinement of the structure. This space group imposes crystallographic C_{3h}-3/m site symmetry on each of the two equivalent molecules in the unit cell. The two mirror-related thiocarbonyl ligands lie on the 3-fold axis, and each of the 3-fold-related Cp rings is bisected by the horizontal mirror plane in two rotationally disordered orientations related by a noncrystallographic 2-fold axis.

The position of the independent nickel atom was located by direct methods, and the other non-hydrogen atoms were determined by successive difference Fourier maps. The ring carbon atoms in each of the two disordered orientations of the half-independent Cp ligand were treated as a rigid group in a manner similar to that used to define the Cp′ ligands for **3**. The site occupancy factors of the two disordered orientations refined to 83% for one ring and 17% for the other. All non-hydrogen atoms, including the carbon atoms in the disordered Cp ring, were refined anisotropically. A final electron-density difference map showed no residual electron density peaks greater than 1.0 eln/Å^3.

Results and Discussion

Structural Features. (a) General Comments. X-ray crystallographic studies of both the Cp′–trinickel clusters and their unsubstituted Cp analogues have provided complementary structural information. Each trinickel cluster is composed of a central nickel triangle with each nickel atom coordinated to either a methylcyclopentadienyl or a cyclopentadienyl ligand. The nickel triangle is capped on each side by two triply bridging carbonyl ligands (**1**, **1a**), two triply bridging thiocarbonyl ligands (**3**, **3a**), or one triply bridging carbonyl and one triply bridging thiocarbonyl ligand (**2**, **2a**). Our general preference for carrying out structural determinations of triangular metal clusters containing noncylindrical Cp′ ligands instead of cylindrical Cp ligands is based on previous work[39] which revealed that the Cp′-containing geometries have a smaller likelihood of possessing crystallographically imposed C_{3h}-3/m symmetry (i.e., an averaged structure involving possible crystal disorder). However, our hope to obtain more precise structural information from X-ray diffraction studies of the Cp′-containing **2** and **3** was only partially realized. Whereas $Ni_3Cp'_3(\mu_3\text{-}CS)(\mu_3\text{-}CO)$ (**2**) has a crystal-ordered structure, its unsubstituted Cp analogue, $Ni_3Cp_3(\mu_3\text{-}CS)(\mu_3\text{-}CO)$ (**2a**), is badly disordered. On the other hand, $Ni_3Cp'_3(\mu_3\text{-}CS)_2$ (**3**) suffers from a serious packing disorder, while its unsubstituted Cp analogue, $Ni_3Cp_3(\mu_3\text{-}CS)_2$ (**3a**), does not.

(b) $Ni_3Cp'_3(\mu_3\text{-}CS)(\mu_3\text{-}CO)$ (2). This trinickel cluster is composed of a central nickel triangle with each nickel atom bound to a Cp′ ligand. The nickel triangle is capped on one side by a triply bridging carbonyl and on the other side by a triply bridging thiocarbonyl ligand. While the $Ni_3(CS)(CO)$ core approximates C_{3v} geometry, the entire molecule possesses crystallographic C_1-1 site symmetry (Figure 1). The Ni–Cp′ bonding in each of the three independent Cp′ rings is similarly asymmetrical; the distance from the nickel atom to the cyclopentadienyl ring carbon atom bonded to the methyl carbon is 0.04–0.05 Å longer than the average distance from the nickel atom to the two carbon atoms on the opposite side of each of the three rings. The methyl substituents of the three Cp′ ligands are each oriented toward the capping CS ligand. The nearest CH···S contact of 3.29 Å indicates that no unusual interactions are occurring.

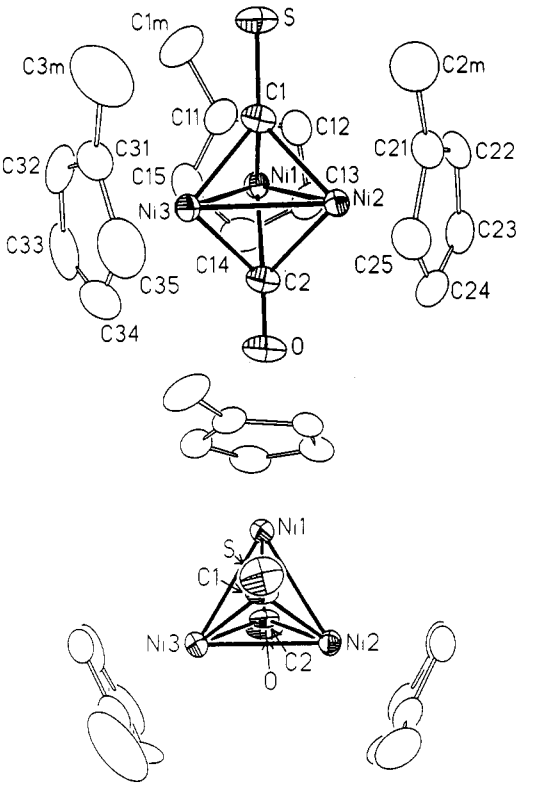

Figure 1. Two views of the crystal-ordered 49-electron $Ni_3Cp'_3(\mu_3\text{-}CS)(\mu_3\text{-}CO)$ (**2**), which has crystallographic C_1-1 site symmetry and pseudo-C_{3v}-3m symmetry. Atomic thermal ellipsoids are drawn at the 30% probability level.

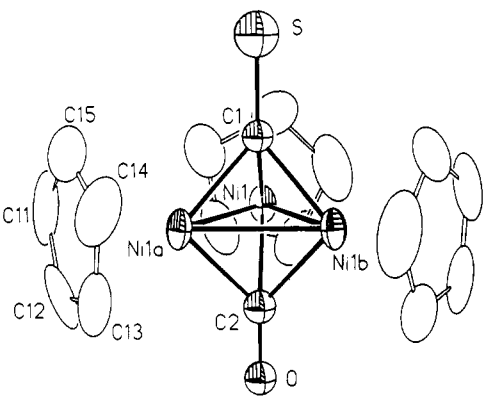

Figure 2. View of the crystal-disordered 49-electron $Ni_3Cp_3(\mu_3\text{-}CS)(\mu_3\text{-}CO)$ (**2a**), which has crystallographic C_3-3 site symmetry. Only one orientation of the disordered CS and CO capping ligands is shown. Atomic thermal ellipsoids are drawn at the 25% probability level.

(c) $Ni_3Cp_3(\mu_3\text{-}CS)(\mu_3\text{-}CO)$ (2a). Under the noncentrosymmetric space group $P6_3$, the molecular structure of **2a** possesses C_3-3 site symmetry, which crystallographically imposes an equilateral triangle of nickel atoms. The basic molecular structure is similar to that observed for **2**; however, the positions of the capping CS and CO ligands are disordered via a pseudo-mirror-plane reflection across the trinickel plane with nonequivalent occupancy factors (viz., 0.25 and 0.75) on both sides of the nickel triangle.

(39) Pulliam, C. R.; Thoden, J. B.; Stacy, A. M.; Spencer, B.; Englert, M. H.; Dahl, L. F. *J. Am. Chem. Soc.* **1991**, *113*, 7398–7410 and references therein.

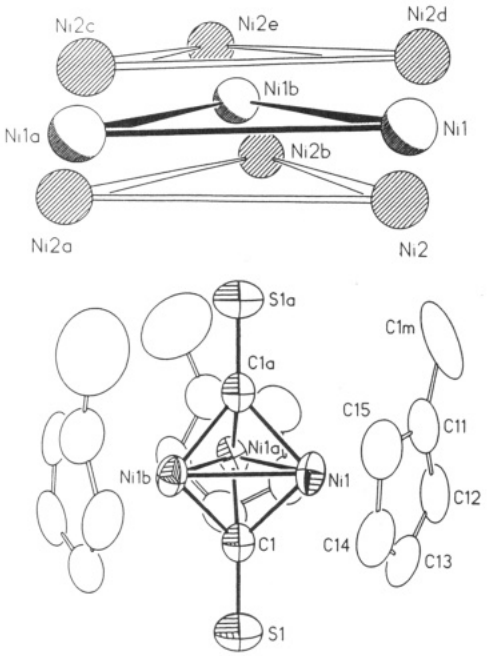

Figure 3. (a) Isotropic model of the orientational disorder of the trinickel core of $Ni_3Cp'_3(\mu_3\text{-}CS)_2$ (**3**), which has crystallographic D_3-32 site symmetry. The major orientation (ca. 80%) of the equilateral nickel triangle has one independent position, Ni1. Two 2-fold-related minor orientations (each ca. 10%) of the equilateral nickel triangle are located above and below the major orientation; the one independent position, Ni2, is approximately 0.5 Å from the Ni1 position. (b) View of the crystal-averaged structure of the 49-electron $Ni_3Cp'_3(\mu_3\text{-}CS)_2$ (**3**), which was refined anisotropically; the resulting size, shape, and orientation of the thermal ellipsoid of the independent nickel atom (and that of each other non-hydrogen atom) thereby approximates the solid-state orientational disorder of **3**. Only one orientation of each Cp′ ring rotationally disordered by a horizontal crystallographic 2-fold axis is displayed. Atomic thermal ellipsoids are drawn at the 20% probability level to provide clarity.

Although reliable positions for the CS and CO ligands could not be determined from difference Fourier maps, fixing them in idealized positions provided a reasonably good structural refinement. The abnormally large anisotropic thermal parameters of the Cp carbons (Figure 2) indicate the presence of considerable ring libration and/or orientational crystal-disorder of the Cp rings.

(d) $Ni_3Cp'_3(\mu_3\text{-}CS)_2$ (3). The $Ni_3(CS)_2$ core of **3** possesses D_3-32 site symmetry with an equilateral triangle of nickel atoms capped on both sides by a triply bridging thiocarbonyl ligand. A crystal-packing disorder is present involving one major (~80%) and two equivalent minor (each ~10%) molecular orientations within the unit cell. This orientational disorder is illustrated in Figure 3a with the major nickel position labeled Ni1 and the 2-fold-related minor positions labeled as Ni2. Difference Fourier maps revealed crystal-disordered nickel triangles above and below the major trinickel configuration. Each of the latter disordered molecules is rotated slightly about the crystallographic 3-fold axis with the equivalent distances between the major independent nickel position and each of the disordered nickel positions being ca. 0.5 Å. Figure 3b shows the averaged structure of the entire molecule refined anisotropically. The effect of this orientational disorder is clearly evident from the canted elongation of the nickel thermal ellipsoids, which encompass the electron density represented by the orientationally disordered nickel atoms. In addition to the three different orientations of each Cp′ ligand due to the packing disorder, each ligand is also rotationally disordered by a horizontal crystallographic 2-fold axis passing through each nickel atom.

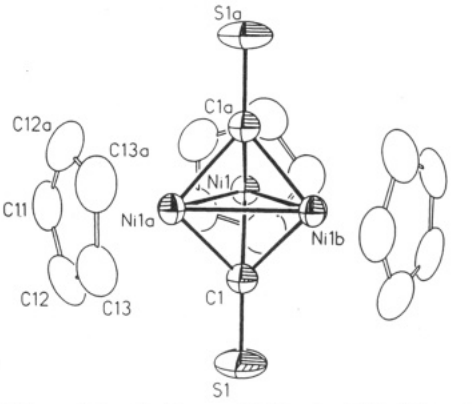

Figure 4. View of the 49-electron $Ni_3Cp_3(\mu_3\text{-}CS)_2$ (**3a**), which has crystallographic C_{3h}-3/m site symmetry. The molecular structure consists of a crystal-ordered $Ni_3(CS)_2$ core. The independent Cp ring possesses a horizontal noncrystallographic 2-fold-related rotational disorder with refined occupancy factors of 83% and 17%; the disordered Cp rings are shown for only the major orientation. All atomic thermal ellipsoids are drawn at the 30% probability level.

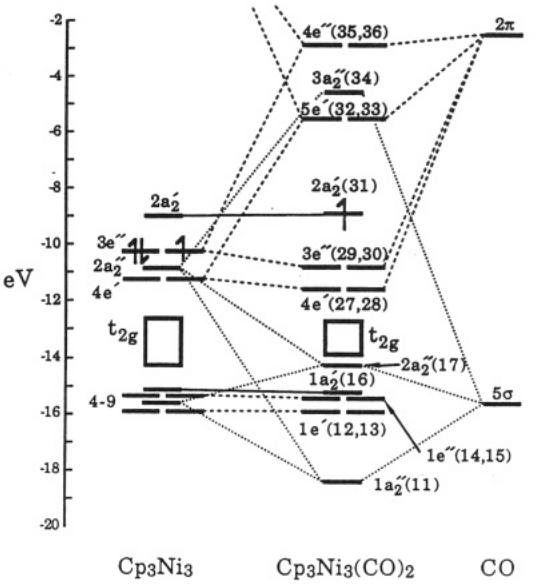

Figure 5. Correlation diagram for selected MOs of the 49-electron Fischer–Palm $Ni_3Cp_3(\mu_3\text{-}CO)_2$ (**1a**) under D_{3h} symmetry. Large dashed lines represent π-bonding interactions, smaller dashed lines correspond to σ-bonding interactions, and solid lines are drawn to MOs that have no capping ligand contribution.

(e) $Ni_3Cp_3(\mu_3\text{-}CS)_2$ (3a). The molecular configuration of **3a** is similar to that of its disordered Cp′ analogue (**3**). Under crystallographic C_{3h}-3/m site symmetry, the $Ni_3(CS)_2$ core consists of an equilateral nickel triangle symmetrically capped above and below by mirror-related triply bridging thiocarbonyl ligands. The one-half independent Cp ring, bisected by the horizontal mirror plane, has a noncrystallographic 2-fold-related rotational crystal disorder with occupancy factors of 83% and 17%; only the major crystal-disordered orientation is shown in Figure 4. The anisotropic thermal ellipsoids of the Cp carbon atoms reflect librational-like ring motion.

Bonding Analysis. Bonding in **1a**, **2a**, and **3a** takes the same basic form, as is shown in their molecular orbital diagrams (Figures 5–7). The electronic structure is largely determined by the Ni–Cp interactions, which, as shown for Ni_3Cp_3, separate the fragment orbitals into Ni–Cp bonding and antibonding manifolds, and a set of t_{2g}-like nickel orbitals that are essentially Ni–Cp nonbonding.

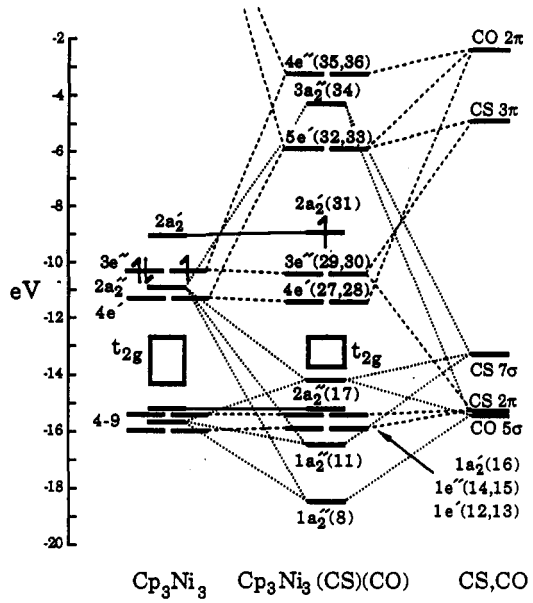

Figure 6. Correlation diagram for selected MOs of the 49-electron $Ni_3Cp_3(\mu_3\text{-}CS)(\mu_3\text{-}CO)$ (**2a**). The MOs are labeled under D_{3h} (instead of C_{3v}) symmetry in order to correlate energy levels with corresponding ones for the D_{3h} **1a** and **3a**. Large dashed lines represent π-bonding interactions, smaller dashed lines correspond to σ-bonding interactions, and solid lines are drawn to MOs that have no capping ligand contribution.

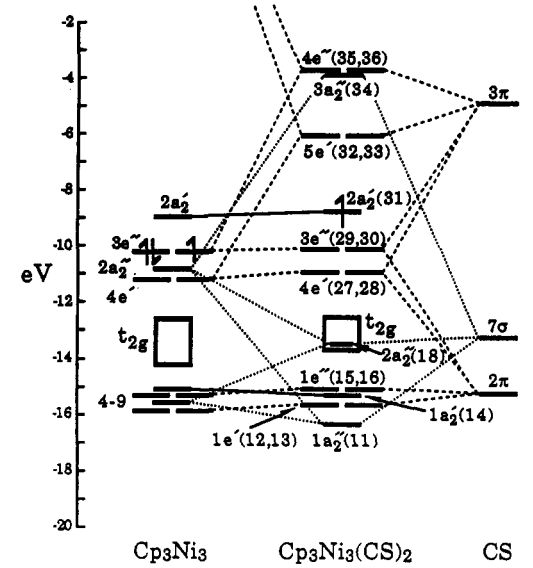

Figure 7. Correlation diagram for selected MOs of the 49-electron $Ni_3Cp_3(\mu_3\text{-}CS)_2$ (**3a**) under D_{3h} symmetry. Large dashed lines represent π-bonding interactions, smaller dashed lines correspond to σ-bonding interactions, and solid lines are drawn to MOs that have no capping ligand contribution.

Interactions of these fragment orbitals with the triply bridging CO and/or CS orbitals to form MOs produce little change in the fragment orbitals of a_2' symmetry (since combinations of triply bridging ligand orbitals with that symmetry cannot be formed); $d_\pi(Ni_3)$–$\pi^*(CX)$ backbonding (X = S, O) between the trinickel symmetry adapted orbitals and the triply bridging ligand $\pi^*(CS)$ and $\pi^*(CO)$ MOs occurs primarily through the higher lying Ni–Cp antibonding 4e′ and 3e″ sets of doubly degenerate orbitals for the Ni_3Cp_3 fragment. Strong σ-like donation from CO or CS lone pair MOs to the Ni_3Cp_3 fragment orbitals of a_2'' symmetry, however, is evidenced by the very large energy separation between the bonding and antibonding combinations.

In each of these 49-electron complexes, the frontier orbitals are the singly occupied $2a_2'$ HOMO, composed primarily of axially symmetric trimetal-antibonding combinations of the in-plane nickel $3d_{xy}$AOs, and the filled 4e′ and 3e″ orbitals of predominantly Ni–Cp antibonding character. Extended Hückel calculations by Hoffmann and co-workers[10] on the then-hypothetical 46-electron $Co_3Cp_3(\mu_3\text{-}CO)_2$[40,41] and $Rh_3Cp_3(\mu_3\text{-}CO)_2$[41c,42,43] produced a set of frontier orbitals similar to those obtained here, as did calculations[41a,44] with the Fenske–Hall model on $Co_3Cp_3(\mu_3\text{-}CO)_2$. Earlier studies of **1a** with the Fenske–Hall model by Rives et al.[11] also predicted the singly-occupied a_2' HOMO but differed significantly from the other studies in placing the 4e′ and 3e″ orbitals below the pseudo-t_{2g} set. As discussed with regard to related calculations[18] for $Ni_3Cp_3(\mu_3\text{-}S)_2$, the 4s and 4p Ni(+1) AOs in the present calculations have been contracted relative to those in the calculations by Rives et al.;[11] hence, the different results reported here reflect the fact that results from the Fenske–Hall method[21] depend on the choice of basis set used.[22]

As is particularly evident from the correlation diagram of **2a** (Figure 6), the occupied 7σ(CS) donor orbital and the unoccupied 3π(CS) acceptor orbital (alternatively designated as the antibonding π^*(CS)) are closer in energy to the corresponding nickel symmetry orbitals (SOs) of the Ni_3Cp_3 fragment than are the corresponding occupied 5σ(CO) donor orbital and the unoccupied 2π(CO) (i.e., antibonding π^*(CO)) acceptor orbitals. In addition, the greatly destabilized, occupied 2π(CS) donor orbitals (alternatively denoted as bonding π(CS)) are sufficiently close in energy that they also interact significantly with the nickel SOs of the Ni_3Cp_3 fragment; in sharp contrast, the much lower energy occupied 1π(CO) (i.e., bonding π(CO)) donor orbitals are essentially nonbonding in this and the other complexes. In the coordination of the capping CS ligand to the trimetal framework, it is important to note the composite effects of these frontier ligand orbitals on the C–S bond energy and bond length. Although these calculations indicate that CO and CS are comparable σ-donors (with the Mulliken orbital populations[45,46] for both the 5σ(CO) and the 7σ(CS) orbitals reduced from 2.00e in the free ligand to 1.34e in **1a**, **2a**, and **3a**), σ-donation via the 7σ(CS) orbital should markedly strengthen the C–S bond due to the 7σ(CS) orbital possessing considerable C–S antibonding character; this trend should give rise to an increased C–S stretching frequency as well as a shorter C–S bond length. On the other hand, the greater π^*-acceptor ability of CS is evidenced by the greater 3π(CS) orbital populations (0.52e for each degenerate orbital in **3a**) than the corresponding 2π(CO) orbital populations (0.42e for

(40) 46-electron $Co_3Cp_3(\mu_3\text{-}CO)_2$: Barnes, C. E.; Orvis, J. A.; Staley, D. L.; Rheingold, A. L.; Johnson, D. C. *J. Am. Chem. Soc.* **1989**, *111*, 4992–4994.

(41) 46-electron $Co_3Cp^*_3(\mu_3\text{-}CO)_2$ (where $Cp^* = \eta^5\text{-}C_5Me_5$): (a) Olson, W. L.; Schugart, K. A.; Fenske, R. F.; Dahl, L. F. *Abstracts of Papers*, 187th National Meeting of the American Chemical Society, St. Louis, MO; American Chemical Society: Washington, DC, 1984; INOR 279. (b) Olson, W. L.; Stacy, A. M.; Dahl, L. F. *J. Am. Chem. Soc.* **1986**, *108*, 7646–7656. (c) Bray, A. C.; Green, M.; Hankey, D. R.; Howard, J. A. K.; Johnson, O.; Stone, F. G. A. *J. Organomet. Chem.* **1985**, *281*, C12–C16.

(42) 46-electron $Rh_3Cp^*_3(\mu_3\text{-}CO)_2$: Green, M.; Hankey, D. R.; Howard, J. A. K.; Louca, P.; Stone, F. G. A. *J. Chem. Soc., Chem. Commun.* **1983**, 757–758.

(43) 46-electron $(MCp^*)_n(CoCp)_{3-n}(CO)_2$ (where M = Co, Rh, Ir; n = 1, 2): (a) Herrmann, W. A.; Barnes, C. E.; Zahn, T.; Ziegler, M. L. *Organometallics* **1985**, *4*, 172–180. (b) Horlein, R.; Herrmann, W. A.; Barnes, C. E.; Weber, C. *J. Organomet. Chem.* **1987**, *321*, 257–272. (c) Barnes, C. E.; Dial, M. R. *Organometallics* **1988**, *7*, 782–784. (d) Barnes, C. E.; Dial, M. R.; Orvis, J. A.; Staley, D. L.; Rheingold, A. L. *Organometallics* **1990**, *9*, 1021–1035.

(44) Olson, W. L.; Dahl, L. F. *J. Am. Chem. Soc.* **1986**, *108*, 7657–7663.

Table V. Comparison of Mean Distances (Å) for the $Ni_3(\mu_3\text{-}X)(\mu_3\text{-}Y)$ Core Geometries in the 49-Electron $Ni_3Cp'_3(\mu_3\text{-}CO)_2$ (1), the Fischer–Palm $Ni_3Cp_3(\mu_3\text{-}CO)_2$ (1a), $Ni_3Cp'_3(\mu_3\text{-}CS)(\mu_3\text{-}CO)$ (2), $Ni_3Cp_3(\mu_3\text{-}CS)(\mu_3\text{-}CO)$ (2a), $Ni_3Cp'_3(\mu_3\text{-}CS)_2$ (3), and $Ni_3Cp_3(\mu_3\text{-}CS)_2$ (3a)

	1[a]	1a[b]	2[c]	2a[c]	3[c]	3a[c]
cryst state[d]	ord	ord	ord	disord	disord	ord
cryst site sym	C_1-1	C_{3h}-3/m	C_1-1	C_3-3	D_3-32	C_{3h}-3/m
pseudo-core sym	D_{3h}	D_{3h}	C_{3v}	C_{3v}	D_{3h}	D_{3h}
Ni–Ni	2.389	2.389 (2)	2.388	2.383 (2)	2.364	2.375 (1)
Ni–CO	1.943	1.932 (9)	1.948	1.97		
Ni–CS			1.918	1.92	1.90	1.922 (7)
C–O	1.175	1.183 (13)	1.163 (3)	1.23		
C–S			1.598 (2)	1.55	1.61	1.539 (11)

[a] Reference 20. [b] Values are from a redetermined least-squares refinement based upon diffractometry data.[9a] [c] This work. [d] Ord denotes ordered structure for the $Ni_3(\mu_3\text{-}X)(\mu_3\text{-}Y)$ core geometry; disord denotes crystal-disordered structure for the $Ni_3(\mu_3\text{-}X)(\mu_3\text{-}Y)$ core geometry.

each degenerate orbital in **1a**). Thus, the CS ligand π^*-backbonding removes 2.08e from the three nickel atoms in **3a**, while CO removes 1.68e through π^*-backbonding from the three nickel atoms in **1a**. The considerably greater trinickel backbonding to the π^*(CS) orbitals is the prime driving force for a uniform shift in electron density from the nickel atoms to the ligand atoms on going from **1a** to **2a** to **3a**. This redistribution of electron density is reflected from an examination of the computed Mulliken atomic charges for these three clusters.[45,46] The loss of electron density from each nickel atom upon substitution of a CS ligand for CO gives rise to an increased nickel positive charge from +0.30 in **1a** to +0.34 in **2a** to +0.37 in **3a**. The Mulliken atomic charges on each CO and CS ligand are observed to be essentially constant in **1a**, **2a**, and **3a**. For CO the C and O charges are −0.01 and −0.16, respectively, while for CS the C and S charges are −0.26 and +0.02, respectively. The large accumulation of negative charge at the thiocarbonyl carbon atom is a composite effect of the greater π^*-acceptor ability of the capping CS ligand and the sulfur atom being less electronegative than the oxygen atom. The larger net charge of −0.24 for each CS ligand versus −0.17 for each CO ligand is also in agreement with CS being a markedly better π^*-acceptor capping ligand than CO. It is noteworthy that each Cp ligand increases slightly in negative charge from −0.19 in **1a** to −0.20 in **2a** to −0.21 in **3a**. Mulliken overlap populations indicate that donation to the nickel SOs from the two π-donor orbitals of each CS ligand in **2a** and **3a** is surprisingly small, which is presumably a consequence of the electron-rich trinickel systems in **2a** and **3a**; a net charge donation of only −0.04e from each degenerate 2π-(CS) orbital is consistent with an orbital population of 1.96e for each 2π(CS) orbital (as compared to that of 2.00e for each low-energy (nonbonding) 1π(CO) orbital) in **2a** and **3a**.

Thus, the dominant effect upon substituting a triply bridging CS ligand for CO is the increased π^*(CS) backbonding interaction, which should produce a stronger trimetal-CS bond and a correspondingly weaker C–S bond. These bonding trends are also consistent with the results of the MO calculations by Lichtenberger and Fenske[24] on the terminal CS ligands in $Cr(CO)_5CS$ and $MnCp(CO)_2CS$. The results of our MO calculations on **1a**, **2a**, and **3a** are presented in conjunction with the correlations obtained from the stereophysical analysis of these thiocarbonyl-capped trinickel clusters (vide infra).

Comparison of Geometries and Resulting Bonding Implications. (a) M–M Distances. A comparison of the mean bond distances found in the 49-electron $Ni_3(X)(Y)$ cores (X, Y = CO or CS) of the Cp′-containing series (**1–3**) and the Cp-containing series (**1a–3a**) is given in Table V. The mean Ni–Ni distance of 2.389 (1) Å in the crystal-ordered $Ni_3(CO)_2$ core of **1** is virtually identical to that in the crystal-ordered $Ni_3(CO)_2$ core of the Fischer–Palm **1a** and to that in the crystal-ordered $Ni_3(CS)(CO)$ core of **2**, where one triply bridging carbonyl has been substituted by a triply bridging thiocarbonyl ligand. The Ni–Ni distance of 2.383 Å determined for the crystal-disordered $Ni_3(CS)(CO)$ core of **2a** is only 0.006 Å shorter. Substitution of the other capping carbonyl ligand by a second thiocarbonyl ligand in the crystal-disordered $Ni_3(CS)_2$ core of **3** and crystal-ordered $Ni_3(CS)_2$ core of **3a** results in small decreases in the mean Ni–Ni distances to 2.364 Å in **3** and 2.375 Å in **3a**. These small but distinct Ni–Ni bond-length shortenings in **3** and **3a** may be attributed mainly to the increased π^*-acceptor capacity of the two capping CS ligands in delocalizing electrons from the out-of-plane trinickel-antibonding e″(d_{yz}) MOs, thereby strengthening the Ni–Ni bonding. Each of these six trinickel clusters either has a crystallographically imposed equilateral nickel triangle (viz., in **1a**, **2a**, **3**, and **3a**) or a pseudoequilateral nickel triangle (viz., in **1** and **2**, which have C_1-1 site symmetry). The relative insensitivity of the mean Ni–Ni distances to substitution of CS for capping CO ligands is consistent with our MO calculations, which show that the frontier orbitals are essentially unperturbed by CS replacement. In addition, the MO calculations predict that CS substitution causes little alteration in the total overlap populations between the nickel atoms, indicating that the Ni-Ni bonding is virtually unchanged. Thus, the calculations are in agreement with the structural results.

(b) Ni–CX and C–X Distances (X = O, S). A comparison of the mean Ni–CO and mean Ni–CS distances in Table V shows the latter to be distinctly shorter. These Ni–CO distances average 1.941 Å for the three structures with ordered CO ligands (**1**, **1a**, and **2**), while the average Ni–CS distance in the two structures with ordered CS ligands (**2** and **3a**) is 1.920 Å. The shorter Ni–CS distances are in accordance with triply bridging CS ligands forming stronger bonds than triply bridging CO ligands to metal atoms in analogous cluster systems. This conclusion is in agreement with X-ray crystallographic and other experimental studies indicating that terminal thiocarbonyl ligands form shorter and hence stronger bonds than terminal carbonyl ligands in the same or corresponding electron-rich mononuclear metal complexes.[12,47,48] Theoretical calculations[23,24] on the "free" CS ligand indicate that this greater

(45) Since the Mulliken scheme, from which atomic charges and orbital populations are obtained on the basis of an equal partitioning of shared electron density, has been criticized as an incorrect prescription,[46] the values of the calculated Mulliken atomic charges and orbital populations are not necessarily realistic but are presented only to indicate trends.

(46) Reed, A. E.; Curtiss, L. A.; Weinhold, F. *Chem. Rev.* **1988**, *88*, 899–926 and references therein.

(47) Andrews, M. A. *Inorg. Chem.* **1977**, *16*, 496–499.

(48) Woodward, S. S.; Jacobson, R. A.; Angelici, R. J. *J. Organomet. Chem.* **1976**, *117*, C75–C80.

metal–thiocarbonyl bond strength arises from CS being both a better π-acceptor and σ-donor ligand than CO; subsequently, it was suggested by Andrews[47] from correlations of the vibrational stretching frequencies of monomeric transition-metal thiocarbonyl complexes with those of their carbonyl analogues that the π^*-acceptor/σ-donor ratio varies more for the CS ligand than for the CO ligand as the electron richness of the metal is varied. Furthermore, Andrews[47] suggested that in electron-rich metal complexes the CS ligand has a higher π-acceptor/σ-donor ratio than the CO ligand but that a crossover occurs in electron-poor systems where the CO ligand has a higher π-acceptor/σ-donor ratio. This trend was experimentally substantiated by Richardson et al.,[49] who observed that the M–CS bond length does indeed become shorter relative to the M–CO bond length as the electron density of the metal increases.

Table V also shows that no significant change in the mean Ni–CO distances occurs on going from the crystal-ordered $Ni_3(CO)_2$ cores of **1** and **1a** to the crystal-ordered $Ni_3(CS)(CO)$ core of **2**. Likewise, no significant change is observed in the mean Ni-CS distances on going from the crystal-ordered $Ni_3(CS)(CO)$ core of **2** to the crystal-ordered $Ni_3(CS)_2$ core of **3a**.

Of prime significance, however, is the observation that the C–S bond length of 1.539 (11) Å in the crystal-ordered $Ni_3(CS)_2$ core of **3a** is 0.06 Å shorter than the C–S bond length of 1.598 (2) Å in the crystal-ordered $Ni_3(CS)(CO)$ core of **2**, which in turn is 0.05 Å shorter than the C–S bond length of 1.646 (3) Å in the crystal-ordered $FeCo_2(CS)S$ core of the 48-electron $(PPh_3)(CO)_2FeCo_2Cp_2(\mu_3\text{-}CS)(\mu_3\text{-}S)$.[16,17] This large C–S bond-length trend is completely consistent with the degree of trimetal back-bonding to an individual π^*-acceptor CS ligand in these three electron-rich thiocarbonylmetal clusters being critically dependent upon the competitive bonding interactions of the other triply bridging ligand—viz., back-bonding to the $\pi^*(CS)$ orbitals being largest for the iron–dicobalt cluster with the π-donor S ligand, intermediate for **2** with the π^*-acceptor CO ligand, and smallest for **3a** with the much better π^*-acceptor CS ligand. These much greater variations in C–S bond lengths than those in C–O bond lengths found for CO-capped metal clusters are also observed for terminal CS ligands[12,47,48] and provide direct experimental evidence substantiating the Fenske–Hall MO results concerning the similar bonding nature of both terminal and bridging CS ligands in electron-rich metal complexes.

Comparison of Spectral–Electrochemical Properties. (a) Infrared Spectral Analysis. Carbonyl and thiocarbonyl IR stretching frequencies for **1–3** and **1a–3a** are summarized in Table I. In the solid state, the ν_{CO} bands of 1735 cm^{-1} for **1** and 1733 cm^{-1} for **1a** are virtually identical. The replacement of one CO ligand by a CS ligand to form **2** from **1** and **2a** from **1a** gives rise to an increase of ca. 30 cm^{-1} in ν_{CO} frequency (viz., to 1763 cm^{-1} for **2** and 1765 cm^{-1} for **2a**); this increase in ν_{CO} frequency is consistent with a better π-accepting CS ligand decreasing the $d_\pi(Ni_3)$–$\pi^*(CO)$ backbonding, even though the C–O bond length does not change significantly (1.175 Å in **1** and 1.163 Å in **2** with ordered CO and CS ligands).

The shift to higher ν_{CO} frequency upon CS substitution for one CO ligand does not hold for the ν_{CS} frequencies. Substitution of the remaining CO ligand by a second triply bridging CS ligand causes ν_{CS} to decrease (instead of increase) from 1128 cm^{-1} in **2** to 1101 cm^{-1} in **3** and from 1135 cm^{-1} in **2a** to 1105 cm^{-1} in **3a**. This frequency change is in contradiction to the C–S bond length decreasing from 1.598 (2) Å in the crystal-ordered $Ni_3(CS)(CO)$ core of **2** to 1.539 (11) Å in the crystal-ordered $Ni_3(CS)_2$ core of **3a**; the substitution of a second better π^*-acceptor CS ligand for the CO ligand results in decreased trinickel back-bonding to the first CS ligand, which gives rise to a significantly shorter C–S bond length in **3a**. This apparent discrepancy of a decrease in CS vibrational frequency when bond length and bonding considerations indicate a strengthening of the C–S bond in the triply bridging thiocarbonyl ligand is analogous to the results of Butler et al.,[50] whose normal-coordinate analysis of vibrational spectra of $M(CO)_5CS$ (M = Cr, W) showed that coupling between the ν(C–S) and ν(M–CS) modes for the terminal thiocarbonyl ligand can give an observed frequency that does not accurately reflect the associated vibrational force constant and bond order of the CS bond.

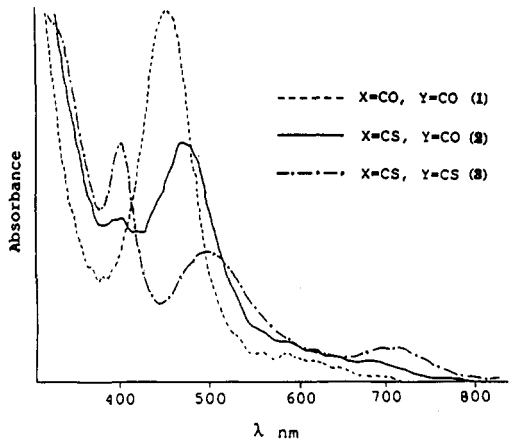

Figure 8. Electronic absorption spectra of the three members (X = Y = CO (1); X = CS, Y = CO (2); X = Y = CS (3)) of the $Ni_3Cp'_3(\mu_3\text{-}X)(\mu_3\text{-}Y)$ series in hexane from 300 to 800 nm.

Fortune and Manning[15] assigned an intense solid-state IR absorption band at 1075 cm^{-1} for $Co_3Cp_3(\mu_3\text{-}CS)(\mu_3\text{-}S)$ and 1069 cm^{-1} for $Co_3Cp'_3(\mu_3\text{-}CS)(\mu_3\text{-}S)$ to the ν_{CS} vibration. These frequencies and the one at 1020 cm^{-1} for $(PPh_3)(CO)_2FeCo_2Cp_2(\mu_3\text{-}CS)(\mu_3\text{-}S)$[16,17] are all lower than the ν_{CS} frequency observed for each trinickel thiocarbonyl complex (**2**, **2a**, **3**, and **3a**). This correlation is consistent with the π-donating triply bridging sulfur atom in each cobalt cluster producing much stronger $\pi^*(CS)$ backbonding, which results in a weaker C–S bond (with lower ν_{CS} frequency) relative to that in each nickel cluster.

(b) Electronic Spectral Analysis. UV–vis spectra of **1–3** are presented in Figure 8. The two major bands present in the visible region for which assignments have been made are shown in Table II. The lower energy band (band A), which occurs as a broad shoulder at ~590 nm in **1**, undergoes a red shift to ~710 nm when CS is substituted for CO in **3**. The higher energy band (band B), found at 456 nm in **1**, also undergoes a red shift to 500 nm with substitution of CS in **3**. The intensity of band B shows a decrease upon each CS substitution, while that of the A band shows a slight increase upon substitution of CS for CO. Relative intensities for spectra in Figure 8 were scaled by setting the highest energy band in the UV region to the same intensity. This band, which occurs at nearly the same wavelength (~220 nm) in each compound, presumably corresponds to transitions between orbitals with no triply bridging ligand character. No attempts were made to assign this and the other UV transitions.

(49) Richardson, Jr., J. W.; Angelici, R. J.; Jacobson, R. A. *Inorg. Chem.* **1987**, *26*, 452–454.

(50) Butler, I. S.; Garcia-Rodriguez, A.; Plowman, K. R.; Shaw III, C. F. *Inorg. Chem.* **1976**, *15*, 2602–2609.

Theoretical calculations allow assignments to be made for band A and band B. Band A is assigned to a transition from the filled doubly degenerate e″ MOs to the partially occupied a_2' HOMO, resulting in a transition from the $^2A_2'$ ground state to a $^2E''$ excited state. The higher energy band B is assigned to excitation of an electron from the filled e′ doubly degenerate MOs (below the previously mentioned e″ orbitals) to the a_2' HOMO, corresponding to a transition from the $^2A_2'$ ground state to a $^2E'$ excited state. Table II compares the observed band energies with the calculated transition energies reported for **1–3**. The calculations indicate that the major effect of substitution of CS for CO is to raise the energies of the filled e″ and e′ MOs relative to that of the a_2' HOMO. While the a_2' HOMO remains unchanged (62% nickel 3d and 36% Cp e_1'' character) upon substituting CS for both CO ligands, the e′ and e″ Ni_3Cp_3 fragment orbitals mix more strongly with both the occupied bonding 2π(CS) (18–20% in $Ni_3Cp_3(\mu_3\text{-}CS)_2$) and the unoccupied antibonding 3π(CS) (14–21% in $Ni_3Cp_3(\mu_3\text{-}CS)_2$) capping ligand orbitals than with the unoccupied antibonding 2π(CO) orbitals (11–16% in $Ni_3Cp_3(\mu_3\text{-}CO)_2$). The tendency to stabilize the Ni_3Cp_3 e′ and e″ levels through increased interactions with the π^*(CS) levels compared with the higher-energy π^*(CO) levels is offset by the greater interactions with the occupied π(CS) levels to give the observed overall increases in energy of the e′ and e″ levels upon substituting a triply bridging CS ligand for CO, as was initially found from Fenske–Hall calculations[24] upon substituting a terminal CS ligand for CO in $Cr(CO)_6$ and $MnCp(CO)_3$ complexes. Thus, the calculated transition energies from these degenerate orbitals to the HOMO show the same red shift observed in the visible spectra. The calculated and observed transition energies agree within ~0.5 eV, which is surprisingly good for the approximate Fenske–Hall method.

(c) ESR Analysis. ESR spectra of the Cp′ species **1–3** show virtually identical line shapes characteristic of an unpaired electron in a nondegenerate orbital with threefold axial symmetry. A single-crystal ESR spectrum of the Fischer–Palm molecule **1a** was initially obtained by Longuet-Higgins and Stone,[4] who suggested from a qualitative bonding model that the unpaired electron resides in an out-of-plane nondegenerate trimetal bonding HOMO. On the basis of a single-crystal ESR investigation of the electonically equivalent $Co_3(CO)_9(\mu_3\text{-}S)$, Strouse and Dahl[5] proposed that the unpaired electron in **1a** occupies an in-plane nondegenerate trimetal antibonding HOMO of a_2'' representation (under D_{3h} symmetry). Theoretical calculations not only support the latter proposal but also show that this MO contains no triply bridging ligand character. This is consistent with the essentially identical values of $g_\parallel = 2.02$ and $g_\perp = 2.10$ (2.11 for **3**) observed for the series **1–3**. With no triply bridging ligand character in the HOMO, ESR spectra would not be expected to vary upon the substitution of a thiocarbonyl ligand for a carbonyl ligand. Hence, it is not surprising that the g values obtained here are essentially identical to those reported for the Fischer–Palm molecule by Longuet-Higgins and Stone.[4]

(d) Mass Spectral Analysis. Positive-ion LD/FT mass spectra provide a substantiation of the compositions of the Cp′-containing **1–3**. Accurate mass determinations and isotope distribution patterns aided in the spectral analysis. Assignments of the major peaks in the positive-ion mass spectra of **1–3** are given in the relevant experimental section. **1** and **2** give rather weak parent ion, $[M]^+$, peaks (m/z 469 and 485, respectively), while in **3** the parent ion corresponds to the base peak (m/z 501).

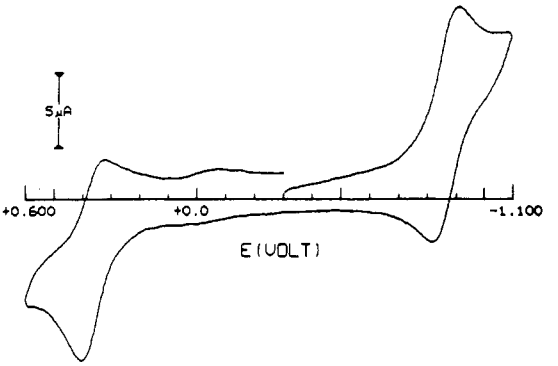

Figure 9. Cyclic voltammogram of $Ni_3Cp'_3(\mu_3\text{-}CS)(\mu_3\text{-}CO)$ (**2**) in CH_2Cl_2 at a scan rate of 200 mV/s. The current–voltage plot displays one reversible reduction wave at $E_{1/2} = -0.86$ V and one reversible oxidation wave at $E_{1/2} = +0.37$ V.

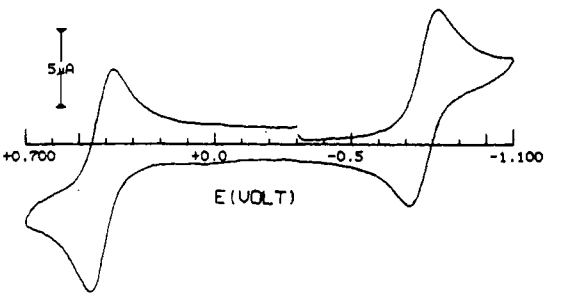

Figure 10. Cyclic voltammogram of $Ni_3Cp'_3(\mu_3\text{-}CS)_2$ (**3**) in CH_2Cl_2 at a scan rate of 200 mV/s. The current–voltage plot displays one quasi-reversible reduction wave at $E_{1/2} = -0.77$ V and one quasi-reversible oxidation wave at $E_{1/2} = +0.42$ V.

Fragment ions corresponding to the successive loss of CO from $[M]^+$ were observed at m/z 441 and 411 in the spectrum of **1**; subsequently, there is further fragmentation with loss of nickel atoms and the Cp′ rings. The positive-ion mass spectrum of **2** also shows ion fragments formed by the loss of a CO ligand (m/z 457) and a CS ligand (m/z 441) from the parent ion. The mass spectrum of **3** displays an ion fragment, $[M - S - 2H]^+$, at m/z 467, corresponding to loss of H_2S from the parent ion. Smaller fragment ions corresponding to the additional loss of Cp′ ligands and nickel atoms are observed. The simultaneous loss of one hydrogen atom per Cp′ ring has also been observed in a mass spectrum of $Ni_2Cp'_2(\mu_2\text{-}CO)_2$[51] and is attributed to the removal of a methyl hydrogen atom, which converts the methylcyclopentadienyl ring into a fulvene ring.

(e) Electrochemical Analysis. Representative cyclic voltammograms (CVs) for **2** and **3** are presented in Figures 9 and 10, respectively. A CV of **1** is given elsewhere.[20,29] These CVs show similar solvent-dependent electrochemical behavior. Each molecular compound exhibits a one-electron oxidation to its 48-electron monocation and a one-electron reduction to its 50-electron monoanion. On the basis of the assignment of the redox couples of **1** as one-electron transfers by Bedard and Dahl,[29] the analogous redox couples of **2** and **3** are also assigned as one-electron processes. A comparison of the $E_{1/2}$ values for the one-electron oxidations and one-electron reductions of **1–3** is given in Table III. The $E_{1/2}$ values show that each substitution of CS for CO makes oxidation more difficult (more positive $E_{1/2}$) and reduction easier (less negative $E_{1/2}$). These trends are in agreement with the notion that CS is a better π-acceptor ligand than CO and is therefore

(51) Byers, L. R.; Dahl, L. F. *Inorg. Chem.* **1980**, *19*, 680–692.

withdrawing more electron density from the trinickel core.

The redox behavior of **1–3** is solvent dependent (Table III). Most notable is that the redox couples of **1** in CH_2Cl_2 are reversible, but in THF they become quasi-reversible. This solvent dependence may account in part for the disagreement in the literature regarding the redox properties of the Fischer–Palm molecule **1a**.[29] The redox behavior of **2** also displays significant solvent dependency; the quasi-reversible oxidation exhibited in CH_2Cl_2 becomes irreversible in THF.

Summary

The solid-state structures of the newly synthesized 49-electron species $Ni_3Cp'_3(\mu_3\text{-}CS)(\mu_3\text{-}CO)$ (**2**), $Ni_3Cp'_3(\mu_3\text{-}CS)_2$ (**3**), $Ni_3Cp_3(\mu_3\text{-}CS)(\mu_3\text{-}CO)$ (**2a**), and $Ni_3Cp_3(\mu_3\text{-}CS)_2$ (**3a**) are compared with the structures of the classic Fischer–Palm molecule, $Ni_3Cp_3(\mu_3\text{-}CO)_2$ (**1a**), and its Cp′ analogue $Ni_3Cp'_3(\mu_3\text{-}CO)_2$ (**1**). The mean Ni–Ni bond lengths remain relatively unaffected by substitution of one or both of the triply bridging carbonyl ligands with triply bridging thiocarbonyl ligands. The structural data for **2** and **3a** provided the first available crystal-ordered M–CS and C–S bond lengths for the μ_3-CS ligand.[13] That the average Ni–CS distance (1.92 Å) in **2** is shorter than the average Ni–CO distance (1.95 Å) indicates that the Ni–CS bond is stronger. This bond-length difference is consistent with the expectation that the capping CS ligand is a better π-acceptor and σ-donor ligand in these electron-rich metal clusters. The cyclic voltammetric data indicate that it is primarily the greater π-accepting ability of the CS ligand that accounts for the trends in the redox potentials. The ESR data are consistent with the results of the molecular orbital calculations, which predict that the unpaired electron in each of these paramagnetic species resides in an in-plane trimetal antibonding HOMO that does not have any triply bridging ligand character. Assignments made for transitions exhibited by the electronic spectra are also in good agreement with those based on the theoretical MO calculations obtained with the Fenske–Hall model.

Acknowledgment. This work was generously supported by the National Science Foundation. We are most grateful to Professor Mary-Ann Pearsall (then, UW—Madison; now, Drew University, Madison, NJ) for her assistance in obtaining UV–vis spectra. We are indebted to EXTREL FTMS (6416 Schroeder Road, Madison, WI) for the use of a FTMS-2000 mass spectrometer.

Supplementary Material Available: Tables of atomic positions and equivalent isotropic thermal parameters, anisotropic thermal displacement coefficients, interatomic distances, bond angles, and data for hydrogen atoms (17 pages). Ordering information is given on any current masthead page.

OM9204595